MALAYSIAN METEOROLOGICAL DEPARTMENT
MINISTRY OF NATURAL RESOURCES AND ENVIRONMENTAL SUSTAINABILITY

Technical Note No. 1/2024

Improved Satellite Rainfall Estimation in Malaysia by Successive Correction

Yip Weng Sang, Fadila Jasmin binti Fakaruddin,
Diong Jeong Yik and
Nursalleh K. Chang @ bin Kasim

TECHNICAL NOTE NO. 1/2024

Improved Satellite Rainfall Estimation in Malaysia by Successive Correction

By

Yip Weng Sang, Fadila Jasmin binti Fakaruddin,
Diong Jeong Yik and
Nursalleh K. Chang @ bin Kasim

Contents

Improved Satellite Rainfall Estimation in Malaysia by Successive Correction

Yip Weng Sang, Fadila Jasmin binti Fakaruddin, Diong Jeong Yik and

Nursalleh K. Chang @ bin Kassim

Abstract

Near-real-time and quantitative rainfall estimation are useful for weather and flood monitoring. The high-resolution satellite rainfall estimation can fulfil this need. It resolves the problems of sparse, unevenly distributed, and erratic rainfall gauge observations. As a country located in the Maritime Continent with extensive interaction between ocean and land across the region, Malaysia is highly vulnerable to extreme weather events such as floods and drought. Therefore, an accurate near-real-time rainfall estimation at high resolution is useful for weather and flood monitoring in Malaysia. This study performs the error analysis of satellite rainfall estimation of the near-real-time precipitation dataset of the Global Satellite Mapping of (GSMaP) and Precipitation Estimation from Remotely Sensed Information Using Artificial Neural Networks-Dynamic Infrared Rain Rate (PDIR) compared to in-situ rainfall gauges over Malaysia. The Barnes successive correction method was evaluated in terms of how well it improved satellite rainfall accuracy in relation to in-situ gauges. It was found that PDIR is more accurate than GSMaP in reference to in-situ gauges. It was also found that the Barnes successive correction further enhanced accuracy of both satellite rainfall datasets in reference to in-situ gauges. Nevertheless, the error between rainfall amounts estimated by satellite and in-situ gauge is still high. This issue can be alleviated by converting rainfall amounts to ranked percentiles. It was found that PDIR corrected by Barnes successive correction (PDIR_C) can attain probability of detection (POD) up to 0.90 out of 1.00 relative to the 95th percentile of gauge rainfall. However, the false alarm ratio (FAR) was also relatively high, that is at least 0.80 out of 1.00, for the 95th percentile of gauge rainfall. Further improvement, for example increasing the gauge density used to train Barnes successive correction, should be considered. In summary, the PDIR_C rainfall estimation was the most accurate in relation to gauge, of all datasets considered in this work.

1.   Introduction

The rainfall amount is an input in rainfall-runoff models for flood forecasting and monitoring land erosion (Devi et al., 2015). Rainfall gauges are the most common instrument to measure rainfall (World Meteorological Organization, 2021a). Although rainfall gauges can be subject to systematic errors, various corrective measures can be used to reduce these systematic errors (Sevruk, 2006). Rainfall gauges are often used to evaluate rainfall estimated by satellite (Sevruk, 2006). Here, rainfall gauges shall be used to evaluate and adjust rainfall estimated by satellite.

Geostationary satellites can observe rainfall at high spatial and temporal resolutions in real-time. In 2018, the World Meteorological Organization (WMO) Space-based Weather and Climate Extremes Monitoring (SWCEM) Demonstration Project invited National Meteorological and Hydrometeorological Services (NHMSs) to validate satellite derived products using rainfall gauge data. The purpose is to monitor extreme events on a short-term basis (World Meteorological Organization, 2022). Among the global satellite-derived products recommended by the SWCEM is the GSMaP dataset. The GSMaP dataset is provided by the Japan Aerospace Exploration Agency (JAXA). The Global Satellite Mapping of Precipitation (GSMaP) with 30 minutes latency estimates rainfall rates using passive microwave measurements (PMW) from low-earth orbiting satellites and infrared (IR) measurements from geostationary satellites (Kubota et al., 2020). Additionally, the PMW algorithm has been adjusted for orographic / non-orographic rainfall (Kubota et al., 2020).

MET Malaysia has been using the GSMaP dataset for near real-time monitoring of hourly rainfall since 2022. Nevertheless, the existence of other satellite rainfall datasets with higher resolution in near real time makes it possible to improve and provide an alternative product to monitor hourly rainfall. One such dataset is the Precipitation Estimation from Remotely Sensed Information Using Artificial Networks (PERSIANN)-Dynamic Infrared Rain Rate (PDIR), (Nguyen et al., 2020). The PDIR dataset has higher spatial resolution than GSMaP with similar latency and temporal resolution (Nguyen et al., 2020). One of the objectives of this study is to determine the near real-time satellite rainfall dataset that is most consistent compared to rainfall gauges.

In our study the Barnes successive correction is used to correct the satellite rainfall estimates. The Barnes scheme was suggested to be computationally efficient, and robust towards strong gradients and areas without data (Grant et al., 2008). Moreover, the Barnes successive correction method does not introduce high frequency noise in the data due to the

possibility of discontinuity in the weighing function (Weymouth et al., 1999). The Barnes scheme was described as highly tunable with accuracy approaching more sophisticated methods (Jones et al., 2009). Additionally, the Barnes scheme does not extrapolate unrealistic values into regions of no data, nor dampen variance (Jones et al., 2009). Numerous works (such as Weymouth et al., 1999; Sinha et al., 2006; Grant et al., 2008; Jones et al., 2009) have used the Barnes successive correction scheme. Weymouth et al. (1999) for instance used the Barnes successive correction to produce near-real-time gridded analyses of rainfall gauges in Australia. Similarly, our aim is also to provide a near real-time national gridded rainfall dataset in Malaysia from the satellite rainfall estimates that have been corrected using rainfall gauges through the Barnes successive correction method.

Before producing a useful and accurate real-time national gridded rainfall dataset from the corrected satellite rainfall estimates, we need to determine which satellite dataset to use. In our understanding, only two (2) high resolution, and near-real-time datasets are currently available, namely the PDIR and GSMaP. Hence, the first objective of this study is to examine the possibility of using PDIR data for near real-time monitoring of hourly rainfall. To do so, we compare the accuracy of PDIR and GSMaP relative to gauge. The second objective is to compare the accuracy of satellite rainfall estimation relative to gauge before and after applying Barnes successive correction. The period of validation, metric of evaluation, description of datasets, and the successive correction methods of Barnes is provided in **Section 2**. In **Section 3**, satellite rainfall estimates are evaluated, and the results of the evaluation are discussed. Finally, **Section 4** the implications of this study are presented.

2.   Data and Methodology

2.1   Period of Verification

The Northeast Monsoon (November – March) is associated with widespread torrential rainfall from cold air outbreaks (Moten et al., 2014). Chen et al. (2013) showed that the period of maximum rainfall in Peninsular Malaysia (west Malaysia) happens from November – December, while the period of maximum rainfall in East Malaysia (North and West Borneo) happens from December – February. Nevertheless, intense rainfall events are also known to occur outside of the usual period of maximum rainfall. For example, the southern Peninsular Malaysia suffered flooding in March 2023 because of heavy rainfall. To evaluate the performance of the PDIR, GSMaP during the NEM, hourly and daily rainfall is evaluated from 01 November 2022 to 01 March 2023 (121 days). These datasets are then corrected with Barnes successive correction scheme (known as corrected PDIR, and corrected GSMaP).

Around three hundred and four (304) rainfall gauges from MET Malaysia were used to validate the efficacy of gridded rainfall and act as input to the Barnes successive correction scheme. Cross-validation is performed over hourly and daily temporal scales to compare the performance of corrected PDIR and GSMaP satellite dataset with their uncorrected counterparts.

List of heavy rainfall events, their type, metrics to evaluate accuracy, and parameters to be evaluated, are summarized in **Table 1**.

<div align="center">Table 1: Summary of Verification</div>

No.	Type	Metric of evaluation	Temporal scale	Parameters evaluated
1	**Seasonal**			
2	**Seasonal** *Categorical rainfall, Slight, Moderate, Heavy, and Intense*	1. **Root mean square error of each station (rmse)** 2. **Pearson correlation coefficient of each station**	**Hourly and Daily Accumulated Rainfall**	1. **GSMaP** 2. **PDIR** 3. **Corrected GSMaP (GSMaP_C)** 4. **Corrected PDIRNow (PDIR_C)**
3.	**Categorical rainfall by percentile**	1. **Probability of Detection (POD)** 2. **False Alarm Ratio (FAR)**		

2.2 Inverse Distance Interpolation using 9-nearest points (IDW-9).

The satellite data are interpolated to gauge location by the method of inverse distance interpolation by nine (9) nearest points. Given gauge g, and set of nine (9) nearest satellite points, $s = \{s_1, s_2, ..., s_9\}$, the satellite rainfall interpolated to gauge g, that is $s(g)$ is described in **Equation 1** below:

$$s(g) = \frac{\sum_{i=1}^{9}\left(\frac{s_i}{d_{s_i}(g)}\right)}{\sum_{i=1}^{9}\left(\frac{1}{d_{s_i}(g)}\right)} \qquad (1)$$

where $d_{s_i}(g)$ is the distance between satellite (*s*) grid point *i* from gauge *g*. Meanwhile, s_i is the satellite rainfall (*s*) estimation at satellite grid point *i*.

2.3   Root mean square error (rmse)

The root mean square error is calculated individually for each gauge, g. The rmse of each gauge is depicted in **Equation 2**:

$$rmse\ (g) = \sqrt{\frac{\Sigma_t(\ Satellite\ rainfall(g,t) - Rainfall(g,t)\ )^2}{\Sigma_t(1)_g}} \quad (2)$$

where *satellite rainfall(g,t)* is the satellite rainfall estimation interpolated (IDW-9) to rainfall gauge (g) at time *t*. Meanwhile, *Rainfall (g,t)* is the rainfall measured at rainfall gauge (g) at time t. The total number of time steps of rainfall gauge (g) is given by $\Sigma_t(1)_g$. Time t refers to each time step during the season.

2.4   Pearson correlation coefficient

The Pearson correlation coefficient is calculated individually for each gauge during seasonal validation. The correlation of each gauge is depicted in **Equation 3**:

$$P(g) = \frac{\Sigma_t\left((Satellite\ rainfall\ (g,t) - \overline{Satellite\ rainfall\ (g)_t}) \times (Rainfall(g,t) - \overline{Rainfall(g)_t})\right)}{\sqrt{\Sigma_t(Satellite\ rainfall\ (g,t) - \overline{Satellite\ rainfall\ (g)_t})^2\ \Sigma_t(Rainfall\ (g) - \overline{Rainfall(g)_t})^2}} \quad (3)$$

where *P(g)* is the Pearson correlation coefficient at gauge g, *Satellite rainfall (g,t)* is the satellite rainfall estimation interpolated (IDW-9) to rainfall gauge (g) at time t, and $\overline{Satellite\ rainfall(g)_t}$ is the time-averaged satellite rainfall estimation interpolated (IDW-9) to rainfall gauge (g). Time t refers to each time step during the season at rainfall gauge (g). Meanwhile, *Rainfall (g,t)* is the rainfall measured by rainfall gauge (g) at time t, and $\overline{Rainfall(g)_t}$ is the time-averaged rainfall measured by rainfall gauge (g). The Pearson correlation coefficient (p) measures the joint covariance between two variables. Only Pearson correlation significant at the 95% level is displayed in this study. The significance test was done by bootstrapping. In addition, a minimum sample size of 29 is considered before the Pearson correlation coefficient is calculated. The minimum sample size of 29 is required to

detect correlation coefficient of at least 0.5 with alpha of 0.05 and power of 80.0%, and alternate hypothesis that the correlation coefficient is different from $R_o = 0$ (Bujang & Baharum, 2016).

2.5   Categorical Validation

The RMSE and Pearson correlation coefficients focuses on rainfall amount (mm). The RMSE informs by how much mm of rainfall amount satellite measurement deviates from the gauge rainfall. Meanwhile, the Pearson correlation describes the linear relationship between rainfall amount (mm) of satellite with gauge.

However, another way to evaluate how well satellite rainfall can pick up gauge rainfall, is through categorical validation. This accounts for the possibility that satellites cannot measure the exact rainfall amount as measured by gauges. Roberts and Lean, (2008) validated a numerical weather prediction (NWP) model by categorizing rainfall amounts using percentiles. In categorical validation, each rainfall value is ranked and converted to percentile. Next, a rainfall event is defined based on a threshold. One hundred (100) rainfall events are defined based on percentiles one (1) to one hundred (100). A rainfall event is said to occur when the rainfall amount exceeds or is equal to the percentile defined for that rainfall event. Hits are the number of rainfall events observed by gauge and picked up by satellite. Misses are number of rainfall event observed by gauge but not picked up by satellite. False alarms are non-rainfall events observed by gauge that are incorrectly classified as rainfall events by satellite.

The hits, misses and false alarms are used to calculate the Probability of Detection (POD) and False Alarm Ratio (FAR). The POD measures the proportion of rainfall events observed by gauge that are correctly picked up by satellite. The FAR measures the proportion of satellite detected rainfall events that are false alarms. The contingency table (Table 2) used to calculate POD (Equation 4) and FAR (Equation 5) are as follows:

Table 2: Contingency table

		Gauge		
		Yes	No	Total
Satellite	Yes	Hits	False Alarms	satellite yes
	No	Miss	True Negative	satellite no
		gauge yes	gauge no	

5

$$POD = \frac{hits}{hits + miss} = \frac{hits}{gauge\ yes} \quad (4)$$

$$FAR = \frac{false\ alarms}{false\ alarms + hits} = \frac{false\ alarms}{satellite\ yes} \quad (5)$$

2.6 GSMaP Satellite Rainfall Estimation

The rainfall estimated by GSMaP is based on merged PMW-IR (Kubota et al., 2020). The PMW algorithm is corrected for orographic rainfall (Kubota et al., 2020). A thirty (30) minute forward extrapolation is applied on cloud motion vector to generate rainfall estimates at the current hour (Kubota et al., 2020). The GSMaP has a latency of thirty (30) minutes, spatial resolution of 0.1 degrees, temporal resolution of one (1) hour, and measures rainfall in units of mm per hour.

2.7 PDIR Satellite Rainfall Estimation

The rainfall estimated by PDIR is calculated based on infra-red (IR) measurements from geostationary satellites (Nguyen et al., 2020). Rainfall rates are estimates from cloud types that are identified by training *self-organizing feature maps* (SOFMs) using high quality PMW dataset (Nguyen et al., 2020). Additionally, the cloud top precipitation rate (T_b – R) curve is calibrated using monthly rainfall climatology data (Nguyen et al., 2020). The PDIR has latency between fifteen (15) to sixty (60) minutes, spatial resolution of 4km, temporal resolution of one (1) hour, and units of mm per hour.

2.8 Rainfall gauges

The gauges used in this study were maintained by MET Malaysia. Three hundred and four (304) gauges was used to correct satellite rainfall estimates in this study. The gauge data is available in real time at an hourly interval. Each gauge measures the rainfall accumulated in units of millimetres over the past hour. Daily rainfall is the sum of hourly rainfall from midnight to midnight (24 hours) in Malaysian Standard Time (MST). The spatial distribution of gauges used in this study are depicted in **Figures 1**.
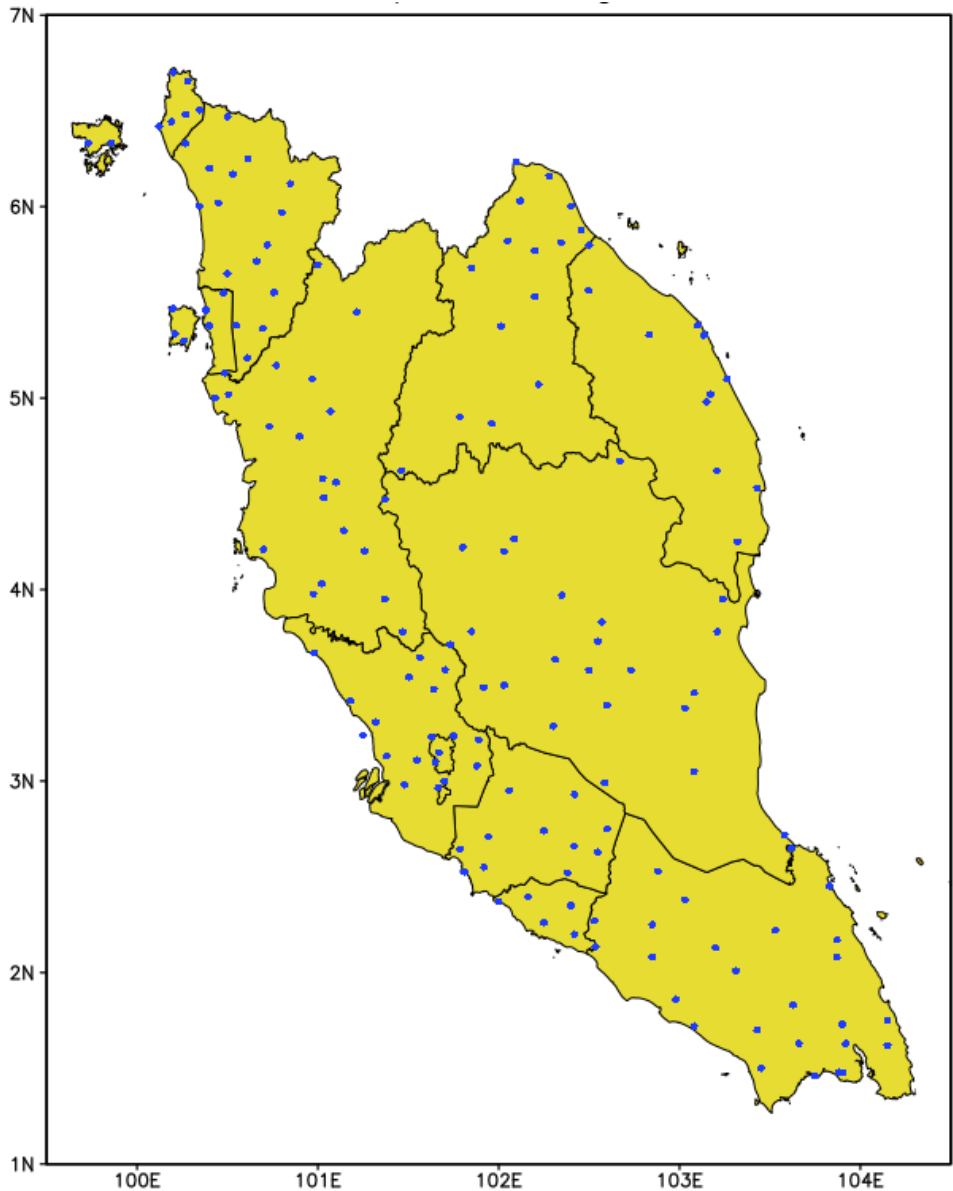
Figure 1a. Spatial distribution of rainfall gauges in Peninsular Malaysia (West Malaysia).
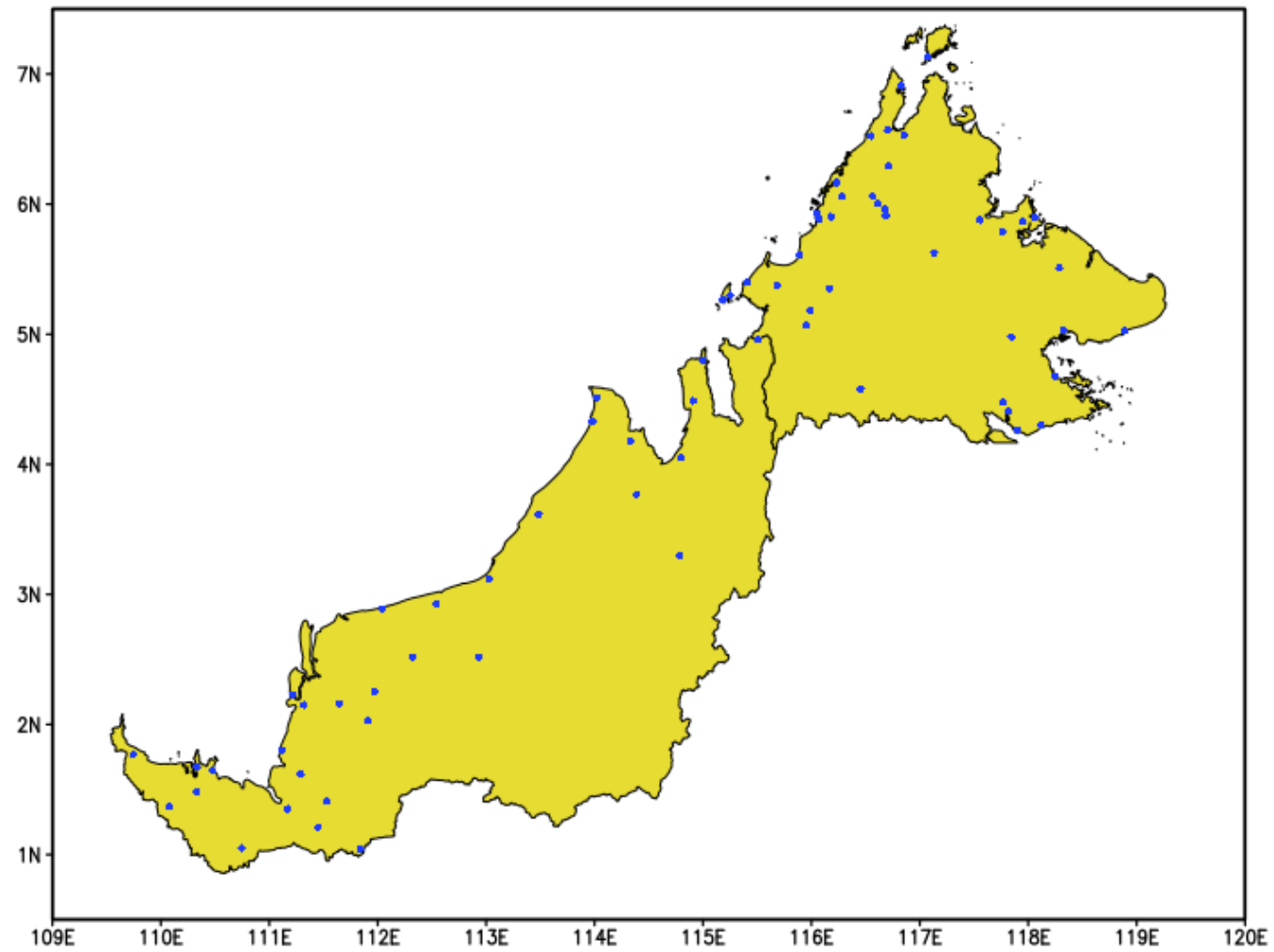
Figure 1b. Spatial distribution of rainfall gauges in Borneo (East Malaysia).

2.9 Barnes successive correction method

The Barnes successive correction method was used to correct satellite gridded rainfall estimation. The satellite gridded rainfall estimation is corrected with respect to MET Malaysia rainfall gauges.

The methodology is succinctly described as follows. Let G denote a set of all rainfall gauges (G) such that $G = \{g_1, g_2, \ldots, g_n\}$. Next, let S denote a set of all satellite rainfall grids (S) such that $S = \{s_1, s_2, \ldots, s_m\}$. First, satellite rainfall grids are interpolated to the position of each rainfall gauges, G, such that $G(S) = \{g_1(s), g_2(s), \ldots, g_n(s)\}$. Here, G(S) is the set of all satellite rainfall estimation (S), interpolated to rainfall gauge location (G). Second, the difference between gauge and satellite is calculated at all gauges (G) where $E(G) = G - G(S) = \{g_1 - g_1(s), g_2 - g_2(s), \ldots, g_n - g_n(s)\}$. Third, $E(G)$ is interpolated back to satellite grid S based on **Equation 6**:

$$e(s) = \frac{\sum_i W_i(s)(g_i - g_i(s))}{\sum_i W_i(s)} \quad (6)$$

where *e(s)* is the difference between gauge and satellite interpolated back to satellite grid point (s). Subscript *i* is rainfall gauge identifier, while W_i (s) is the weight assigned to rainfall gauge *i*. The variable g_i is the rainfall amount measured at rainfall gauge *i* and variable *gᵢ(s)* is rainfall amount measured by satellite at location of gauge *i*. The weight, W_i *(s)* can be represented in **Equation 7**.

$$W_i(s) = \begin{cases} 0 \text{ if } D_R > d_i \\ \exp\left(-4 \times \frac{d_i^2(s)}{D_R^2}\right) \text{ otherwise} \end{cases} \quad (7) \text{ for Barnes Successive Correction}$$

where D_R is the search radius, which is the distance from satellite grid point *s*, containing all gauges *i* used to correct the satellite grid point *s*. Meanwhile, *dᵢ (s)* is the distance between gauge *i* and satellite grid point *s*, and W_i (s) is the Barnes weight as a function of distance between gauge *i* and satellite grid point *s*, within search radius D_R.

Finally, $E(S) = \{e(s_1), e(s_2) \ldots, e(s_m)\}$ which is the interpolated difference of gauge and satellite is used to correct the satellite grid, $S = \{s_1, s_2, \ldots, s_m\}$ as follows:

$$Corrected\ satellite\ grid, S_{corrected} = S + \alpha E(S); \alpha = 0.20 \quad (8)$$

9

where S is the satellite grid, α is a smoothing factor which helps the correction field $E(S)$ adjust satellite rainfall field S smoothly. Since we are repeating the calculation over successively smaller search radii to obtain more localized details, α is important to prevent over-adjusting S. The initial search radius is 45km. It is approximately the average distance between rainfall gauges used in the operational version of PDIR_C, in Malaysia. The subsequent search radius is 35km, 25km, 15km, and 10km The PDIR (GSMaP) dataset which has been corrected by Barnes successive correction is referred to as PDIR_C and GSMaP_C from now on.

2.10   Cross-validation

The ten-fold cross-validation is used throughout this study. It is the most common method of evaluation in machine learning and data mining (Refaeilzadeh et al., 2016). Our dataset was already ordered by increasing latitude and longitude. To increase the spatial coverage of all subsets within our dataset, we randomly re-ordered our dataset once. This is performed before applying ten-fold cross validation.

Next, the randomly re-ordered rainfall gauge data is divided into ten (10) equally (nearly equally) sized subsets. Successive correction is performed using nine (9) of the subsets while one (1) excluded from the successive correction process. The one (1) dataset is also known as the hold-out dataset, which does not participate in generating the successive correction gridded field. In this study, each subset is used in training and separately held-out for validation at least once.

The advantage of ten-fold cross validation is that the validation result is an acceptable estimate of validation result for *unseen* dataset, or dataset outside of that used in this study. The validation result of ten-fold cross-validation can generalize better to full *unseen* dataset because 90% of the data has been used to generate the successive correction field (Refaeilzadeh et al., 2016).

3.   Results and Discussion

3.1   Seasonal Verification

There are three hundred and four (304) gauges used in this study. Each gauge has a corresponding satellite, and corrected satellite, measurement interpolated to the gauge location using IDW-9. For seasonal verification, the rmse and correlation is calculated across time, individually for each 304 gauges, hourly and daily rainfall. The rmse and correlation for each gauge across time (01 November 2022 until 01 March 2021; 121 days) is analysed in **Table 3**, **Figures 2** (rmse), and **Figures 3** (correlation).

Table 3. Summary of boxplots given in **Figures 2** and **3**. Shaded rows (*the best accuracy in relation to gauge*) indicate median, lowest (highest) rmse (correlation). The shaded rows also indicate lowest interquartile range (IQR). The quartiles are calculated based on seasonal rmse and correlation of satellites in relation to gauge.

Time	Dataset	rmse		correlation	
		IQR	Median	IQR	Median
Hourly	GSMaP	1.61	2.94	0.13	0.12
	PDIR	1.27	2.64	0.16	0.24
	GSMaP_C	1.36	2.48	0.19	0.24
	PDIR_C	1.23	2.36	0.19	0.34
Daily	GSMaP	16.0	22.0	0.29	0.40
	PDIR	10.6	18.7	0.33	0.43
	GSMaP_C	10.3	16.9	0.29	0.53
	PDIR_C	8.5	15.2	0.29	0.57

Based **Table 3**, over the entire season, the PDIR dataset has lower rmse and higher correlation than GSMaP. This implies that PDIR rainfall estimates are closer in magnitude to rainfall gauges (lower rmse) and higher joint variability (higher correlation) with rainfall gauges over the entire season. The application of Barnes successive correction further lowers the rmse and increases the correlation for both PDIR and GSMaP. This implies that the Barnes successive correction nudges satellite rainfall grids closer towards rainfall gauge magnitude (lower rmse) and enhances joint variability with rainfall gauges (higher correlation).

The daily rainfall rmse is higher than hourly rainfall rmse because of error accumulation from hourly to daily rainfall. Additionally, the squared error term in the rmse formula penalizes larger errors more than small errors. The daily rainfall correlation is also higher than hourly rainfall correlation. This could happen because the satellite can easily detect ground rainfall over several hours, that may be missed in a single hour.
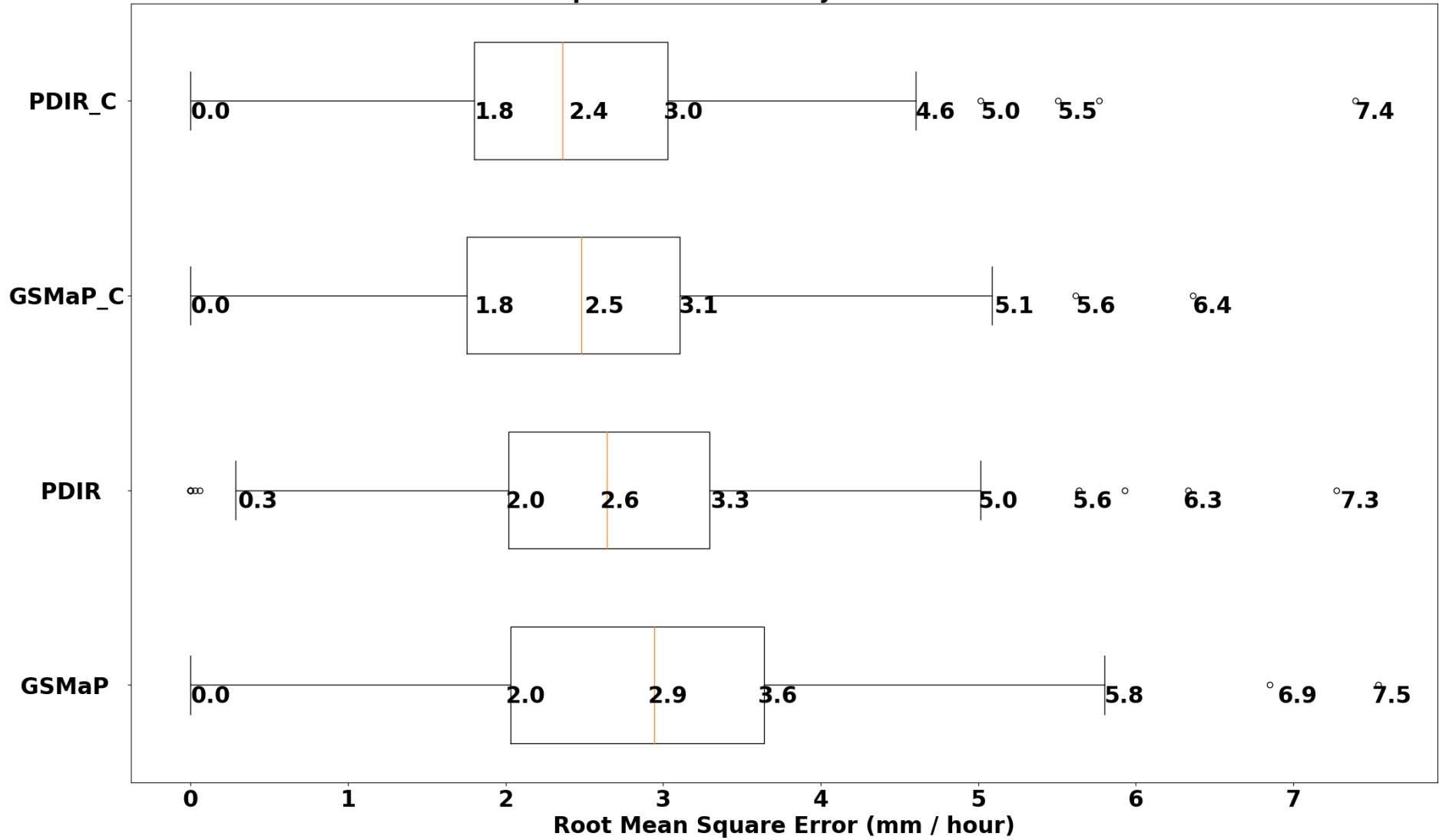
Figure 2a. The rmse of hourly rainfall across the season (01 November 2022 until 01 March 2023.
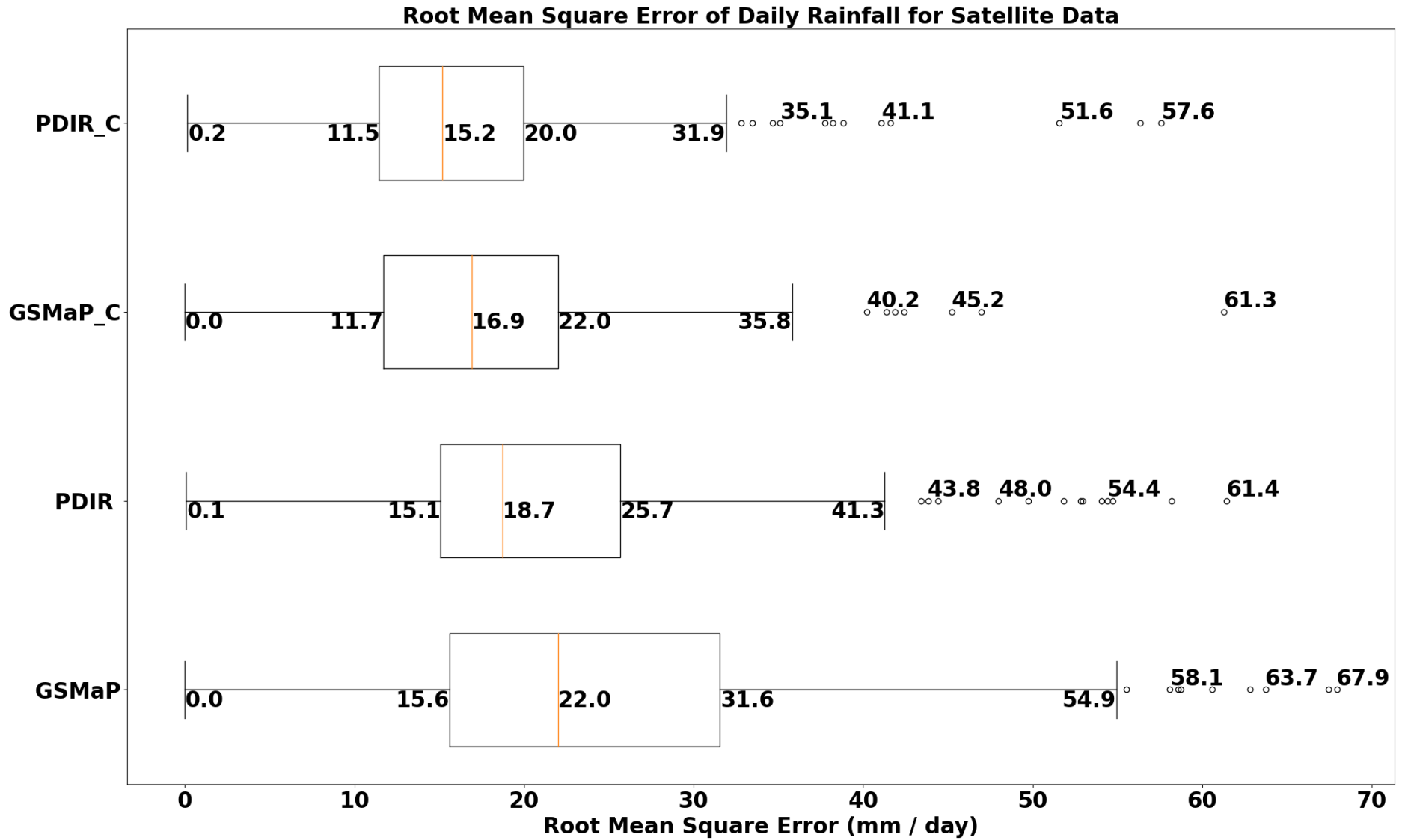
Figure 2b. The rmse of daily rainfall across the season (01 November 2022 until 01 March 2023).
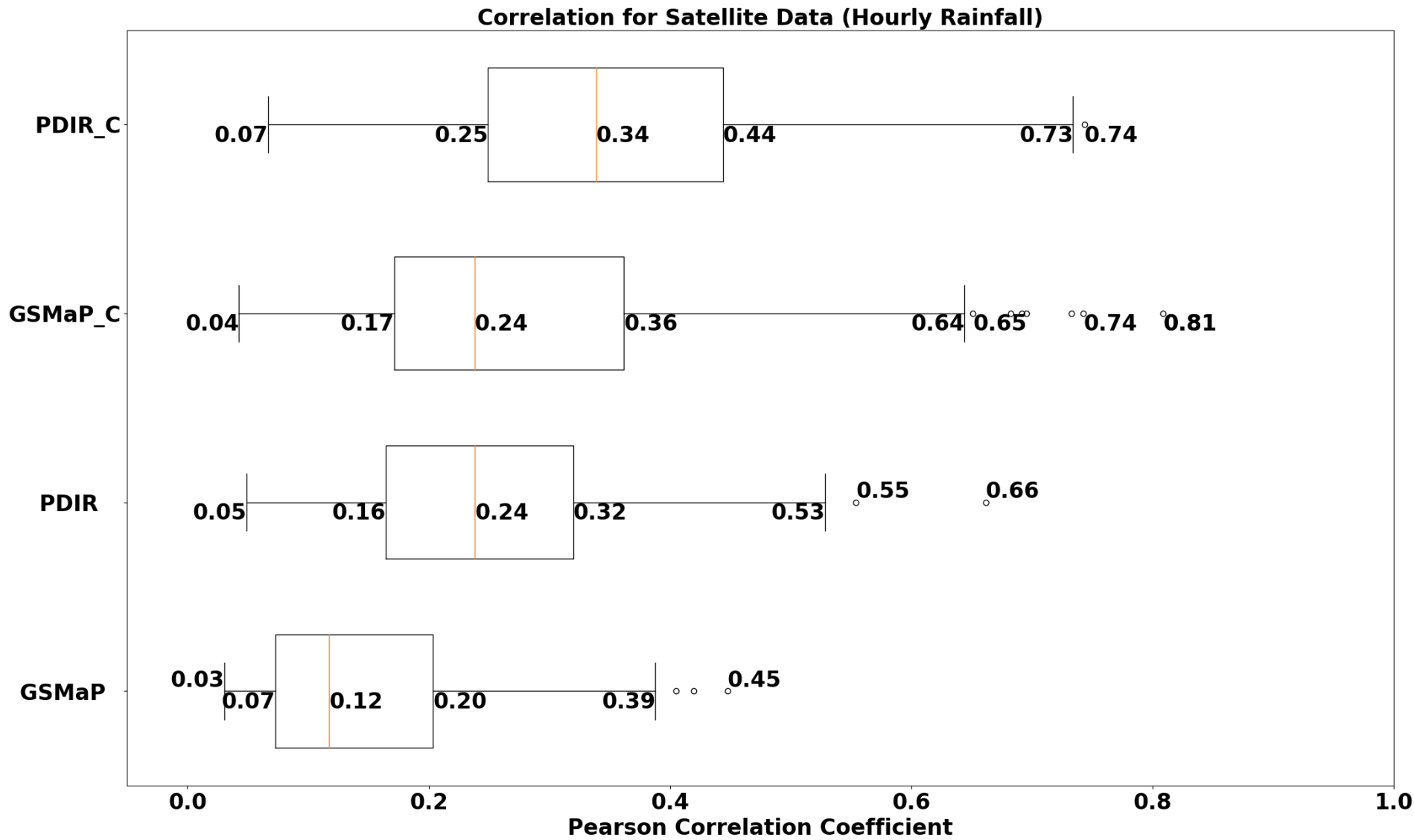
Figure 3a. The correlation of hourly rainfall across the season (01 November 2022 until 01 March 2023).
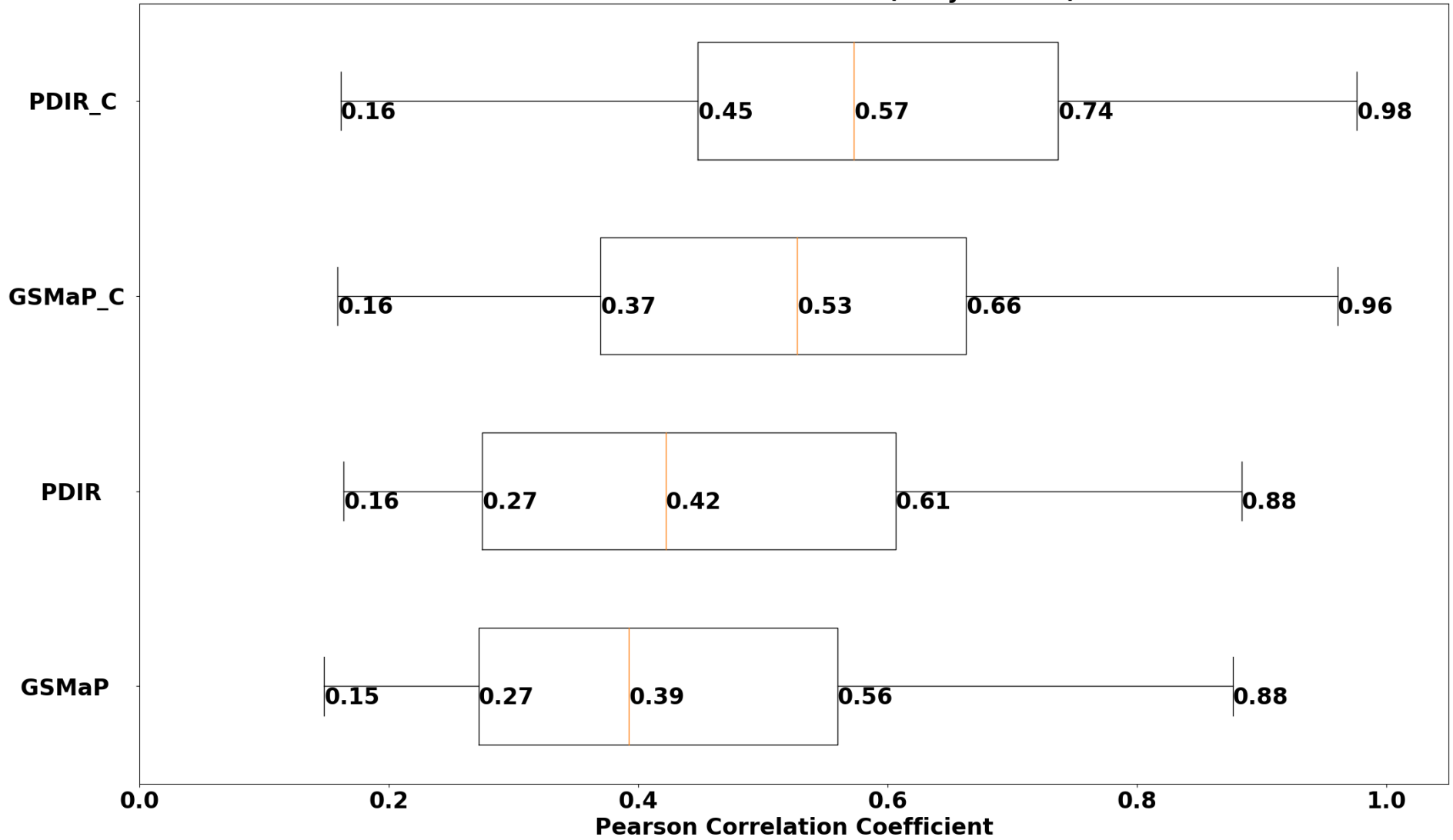
Figure 3b. The correlation of daily rainfall across the season (01 November 2022 until 01 March 2023).

In addition to overall error analysis of seasonal rainfall (01 November 2022 – 01 March 2023), error analysis based on categorical rainfall are performed over the same season. Therefore, the accuracy of PDIR, GSMaP and the effectiveness of Barnes can be evaluated on different categories of rainfall. Hourly rainfall categories are classified based on World Meteorological Organization, 2021b. Meanwhile, the intense, daily rainfall category was defined as greater than or equal to 150mm (Fakaruddin et al., 2020). From here, heavy, daily rainfall category was taken to be greater than or equal to 100 but less than 150mm. Then, moderate, daily rainfall category was taken to be greater than or equal to 50 but less than 100mm. . Rainfall classification in this study is summarized in **Table 4**.

Table 4: Rainfall classification (based on gauge rainfall)

Intensity	Hourly (mm/hour)	Daily (mm/day)
Slight	Less than 2.5	Less than 50
Moderate	Greater than or equal to 2.5, less than 10	Greater than or equal to 50, less than 100
Heavy	Greater than or equal to 10, less than 50	Greater than or equal to 100, less than 150
Intense	Greater than or equal to 50	Greater than or equal to 150

The root mean square error (rmse) of satellite in relation to gauge is calculated for each rainfall classifications (**Figures 4** and **5**). Comparison of the rmse between GSMaP in relation to gauge, and the rmse between PDIR to gauge, is summarized in **Table 5a**. The contents of **Table 5a** are calculated based on **Equation 9a**:

$$P_{rmse}(\%)_{category} = \frac{RMSE_{category}(GSMaP)_{gauge} - RMSE_{category}(PDIR)_{gauge}}{RMSE_{category}(GSMaP)_{gauge}} \times 100\% \quad (9a)$$

where $P_{rmse}(\%)_{category}$ is the percentage of rmse change by rainfall category, $RMSE_{category}(GSMaP)_{gauge}$ is the rmse of GSMaP in relation to gauge for the rainfall category, and $RMSE_{category}(PDIR)_{gauge}$ is the rmse of PDIR in relation to gauge for the rainfall category.

Table 5a: Comparison of rmse (in relation to gauge) between GSMaP and PDIR. Calculation based on **Equation 9a** above. Positive (negative) means GSMaP is less (more) accurate with respect to gauge, compared to PDIR.

	Slight	Moderate	Heavy	Intense
Hourly	-7%	+16%	+9%	+8%
Daily	-5%	+27%	+28%	+24%

For slight rainfall (**Table 5a**), GSMaP has *lower* rmse than PDIR in relation to gauge. In hourly (daily) rainfall, GSMaP has -7% (-5%) *lower* rmse than PDIR. This means that GSMaP is closer to gauge rainfall than PDIR, because it has a smaller rmse in relation to gauge, than PDIR. In short, for slight rainfall, GSMaP is *better* than PDIR, in relation to gauge rainfall amounts.

However, for moderate, heavy, and intense rainfall, instead PDIR is closer to gauge because it has *lower* rmse than GSMaP. Based on **Table 5a**, GSMaP has *more* rmse than PDIR by 16%, 9%, 8% for hourly rainfall, and *more* rmse than PDIR by 27%, 28%, 24% for daily rainfall. This implies that PDIR is closer to gauge rainfall than GSMaP for moderate, heavy, and intense rainfall, because it has *lower* rmse than GSMaP (refer to **Table 5a**) in these categories. In short, PDIR is *better* than GSMaP, for moderate, heavy, and intense rainfall category, in relation to gauge rainfall amounts.

Meanwhile, **Table 5b** and **Table 5c** compares the rmse between satellite and satellite corrected by Barnes successive correction, for each rainfall category. The contents of **Table 5b** and **Table 5c** are based on **Equation 9b**.

$$P_{rmse}(\%)_{corrected} = \frac{RMSE_{corrected\ satellite} - RMSE_{satellite}}{RMSE_{satellite}} \times 100\% \quad (9b)$$

where $P_{rmse}(\%)_{corrected}$ is the percentage change of rmse (relative to gauge) when Barnes successive correction is applied to the satellite, $RMSE_{corrected\ satellite}$ is the rmse of satellite relative to gauge which has been corrected using Barnes successive correction, and $RMSE_{satellite}$ is the rmse of satellite relative to gauge (taken as is, not yet corrected by Barnes successive correction).

Table 5b. Change in rmse (relative to hourly gauge rainfall), after Barnes successive correction. Calculation is based on **Equation 9b**. Negative means Barnes successive correction increases the accuracy of satellite with respect to gauge.

		GSMaP_C	PDIR_C
Hourly	Slight	-20%	-19%
	Moderate	-17%	-9%
	Heavy	-15%	-6%
	Intense	-6%	-4%

Table 5b and **5c** indicates the percentage change in rmse (in relation to gauge) for satellite once Barnes successive correction is applied. **Table 5b** and **5c** shows decreased percentage change (%) that are indicated by negative numbers. The reduction (negative) in rmse (in relation to gauge) seen in **Table 5b** and **5c** indicates that Barnes successive correction reduces the difference between satellites and gauges. This is true for all categories of rainfall.

For example, hourly (**Table 5b**) slight rainfall showed reduction of rmse relative to gauge around -20% for GSMaP_C and PDIR_C. Meanwhile, hourly moderate rainfall showed reduction of rmse relative to gauge by -17% and -9% for GSMaP_C and PDIR_C. For hourly heavy rainfall, around -15% and -6% reduction of rmse relative to gauge was observed in GSMaP_C and PDIR_C. Intense hourly rainfall showed reduction in rmse relative to gauge by of -6% and -4% for GSMaP_C and PDIR_C, when Barnes successive correction is applied.

Table 5c shows the percentage change in rmse (in relation to gauge) for satellite daily rainfall. **Table 5c** is depicted as follows:

Table 5c. Change in rmse (relative to daily gauge rainfall), after Barnes successive correction. Calculation is based on **Equation 9b**. Negative means Barnes successive correction increased the accuracy of satellite with respect to gauge.

		GSMaP_C	PDIR_C
Daily	Slight	-30%	-25%
	Moderate	-23%	-15%
	Heavy	-20%	-13%
	Intense	-31%	-22%

Analysis of daily rainfall (**Table 5c**) shows that, in daily slight rainfall, around -30% (-25%) reduction in rmse relative to gauge, was seen in GSMaP_C (PDIR_C). For moderate daily rainfall, -23% (-15%) reduction in rmse relative to gauge, was seen in GSMaP_C (PDIR_C). For heavy daily rainfall, -20% (-13%) reduction in rmse relative to gauge, was seen in GSMaP_C (PDIR_C). Finally, in intense daily rainfall, reduction in rmse relative to gauge, was -31% (-22%) for GSMaP_C (PDIR_C).

Barnes successive correction is more effective in reducing rmse relative to gauge, for daily rainfall than hourly rainfall. This is shown by the more negative percentage change in **Table 5c** compared to **Table 5b**. PDIR_C showed the least *improvement* in terms of rmse (in relation to gauge) when Barnes successive correction is applied. This is based on less negative percentage values on PDIR_C, than the GSMaP_C column. It implies that PDIR is already closer to gauge rainfall amounts, than GSMaP.

Table 5d shows the average rmse values (units of mm) for each rainfall category and time, in relation to gauge. **Table 5d** is depicted below:

Table 5d: Average root mean square error (rmse) of hourly and daily rainfall by category. Brackets denote standard error of rmse.

Time	Category	Slight	Moderate	Heavy	Intense
Hourly	PDIR_C	1.3 (0.0)	5.1 (0.1)	16.6 (0.2)	55.2 (1.6)
	GSMaP_C	1.2 (0.0)	5.5 (0.1)	17.8 (0.2)	58.1 (1.4)
	PDIR	1.6 (0.1)	5.6 (0.1)	17.7 (0.2)	57.4 (1.5)
	GSMaP	1.5 (0.1)	6.7 (0.2)	19.5 (0.2)	61.9 (1.3)
Daily	PDIR_C	13.1 (0.4)	39.9 (1.1)	70.1 (3.5)	93.8 (7.4)
	GSMaP_C	12.9 (0.4)	50.8 (1.6)	83.0 (3.9)	109.2 (7.8)
	PDIR	17.4 (0.4)	47.9 (1.1)	81.0 (3.9)	119.8 (8.9)
	GSMaP	18.3 (0.6)	66.4 (2.5)	104.1 (5.6)	159.1 (9.6)

The rmse values (mm) increases as rainfall intensity increases. In **Table 5d**, satellite rainfall is not suitable for picking-up intense hourly rainfall. It is because, the lowest rmse (PDIR_C; intense) is more than 50mm per hour, and our definition of intense hourly rainfall is more than 50mm per hour (**Table 4**). A different measure of intense rainfall will be described.
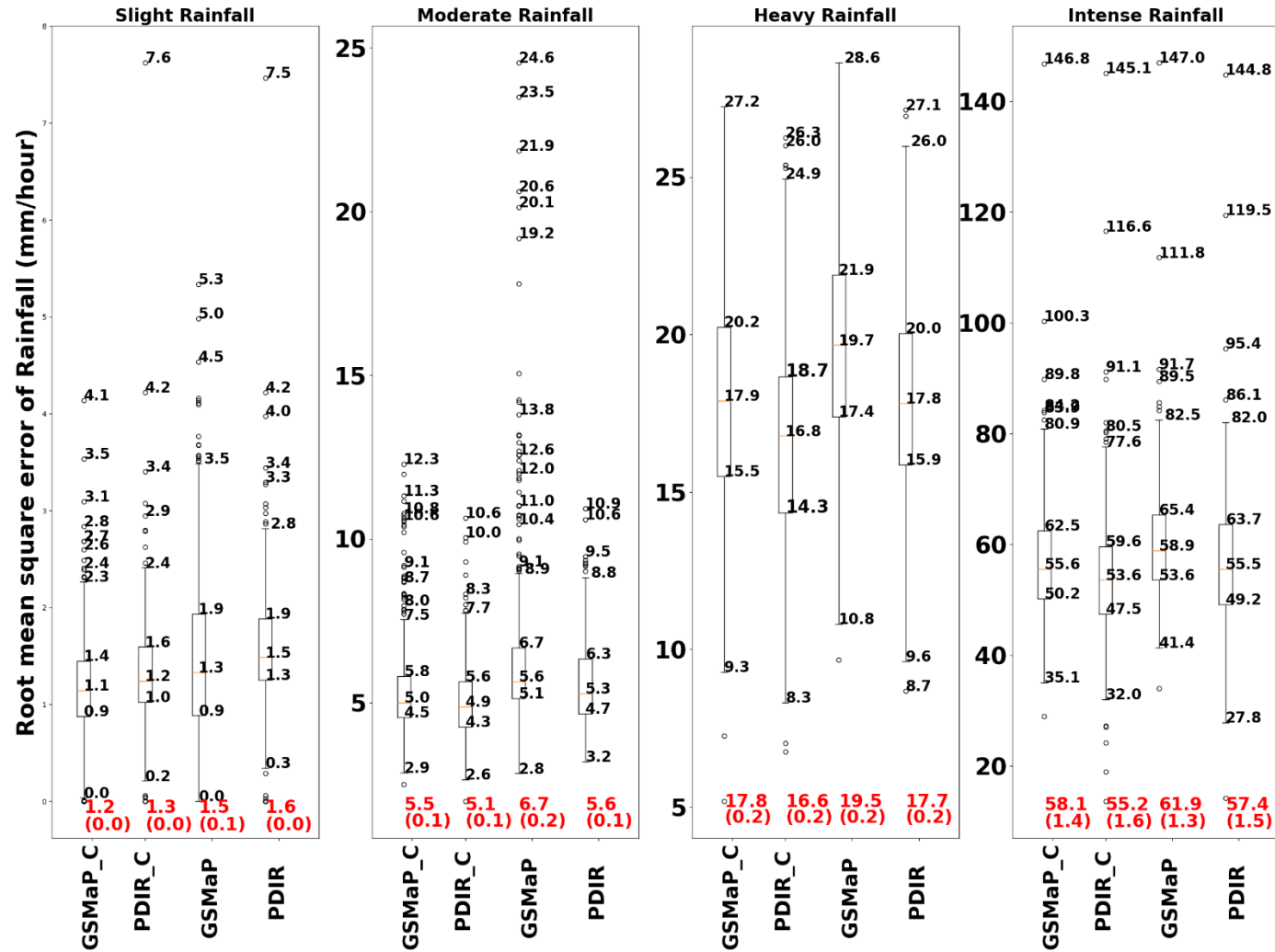
Figure 4. The rmse of hourly rainfall by rainfall classification. Text underneath are average rmse and standard error of rmse (brackets). Refer to **Table 4**, for definition of *slight, moderate, heavy,* and *intense rainfall.*
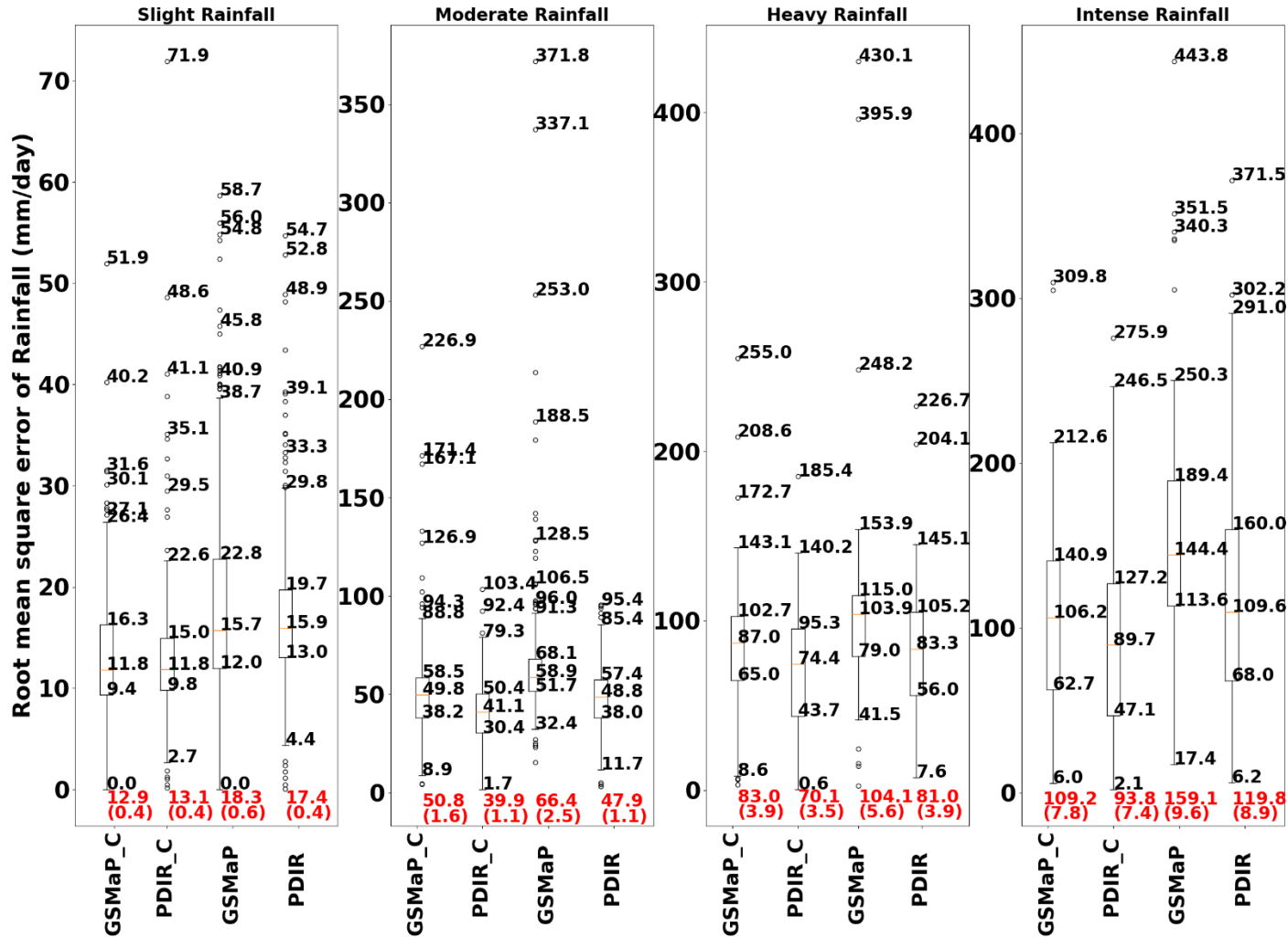
Figure 5. The rmse of daily rainfall by rainfall classification. Text underneath is average rmse and standard error of rmse (brackets). Refer to Table 4. for definition of *slight, moderate, heavy,* and *intense rainfall*.

The correlation coefficient of each rainfall category is shown in **Figure 6**. For intense rainfall, the correlation coefficient was not calculated because the criteria of having at least 29 samples was not fulfilled. Meanwhile, for heavy rainfall events, PDIR has better correlation than GSMaP_NOW. This is obvious when the boxplot of PDIR is around one (1) quartile higher than GSMaP. It implies that PDIR is better than GSMaP, in terms of correlation relative to gauge, during heavy rainfall events recorded at gauge.

For moderate hourly rainfall (**Figure 6**), PDIR continued to show significantly higher correlation relative to gauge, compared to GSMaP. The 75th percentile (top of boxplot) for PDIR has nearly the same correlation as the maximum of GSMaP (top whisker). Meanwhile, the maximum correlation of PDIR (top whisker) is 0.54, which is around half again as high as GSMaP maximum correlation (0.35). The top whisker of the boxplot is the highest datum below the third quartile plus the interquartile range (IQR). Additionally, the median of PDIR is almost equivalent to the 75th percentile (3rd quartile) of GSMaP. It implies that PDIR is nearly one (1) quartile higher correlation, than GSMaP for moderate rainfall.

For slight hourly rainfall (**Figure 6**), there is a small improvement in PDIR (correlation relative to gauge), compared to GSMaP. In this case, the boxplot of PDIR is slightly higher by around 0.02 (correlation) compared to GSMaP. In the coming paragraphs, the impact of Barnes successive correction is discussed.

Barnes successive correction gave the most improvement for GSMaP_C relative to GSMaP. **Figure 6** revealed that for each rainfall category, the boxplot of GSMaP (rightmost) goes up by one quartile when Barnes successive correction is applied (GSMaP_C). For example, in all three rainfall categories, the median GSMaP_C is close to the third quartile of GSMaP. Additionally, the third quartile of GSMaP_C is more than the maximum correlation of GSMaP in heavy and moderate rainfall.

Barnes successive correction also increase correlation for PDIR_C relative to PDIR. In slight rainfall, the correlation (relative to gauge) of PDIR increased by one quartile when Barnes successive correction is applied (PDIR_C). Based on **Figure 6** (slight rainfall), the median of PDIR_C is equal to the third quartile of PDIR. Also, the third quartile of PDIR_C is higher than the third quartile of PDIR, in slight rainfall. Minor improvement of around 0.02 correlation is seen in moderate rainfall, over each quartile of PDIR_C over PDIR. For heavy rainfall, Barnes successive correction increased the maximum, third quartile, and median correlation of PDIR_C over PDIR.
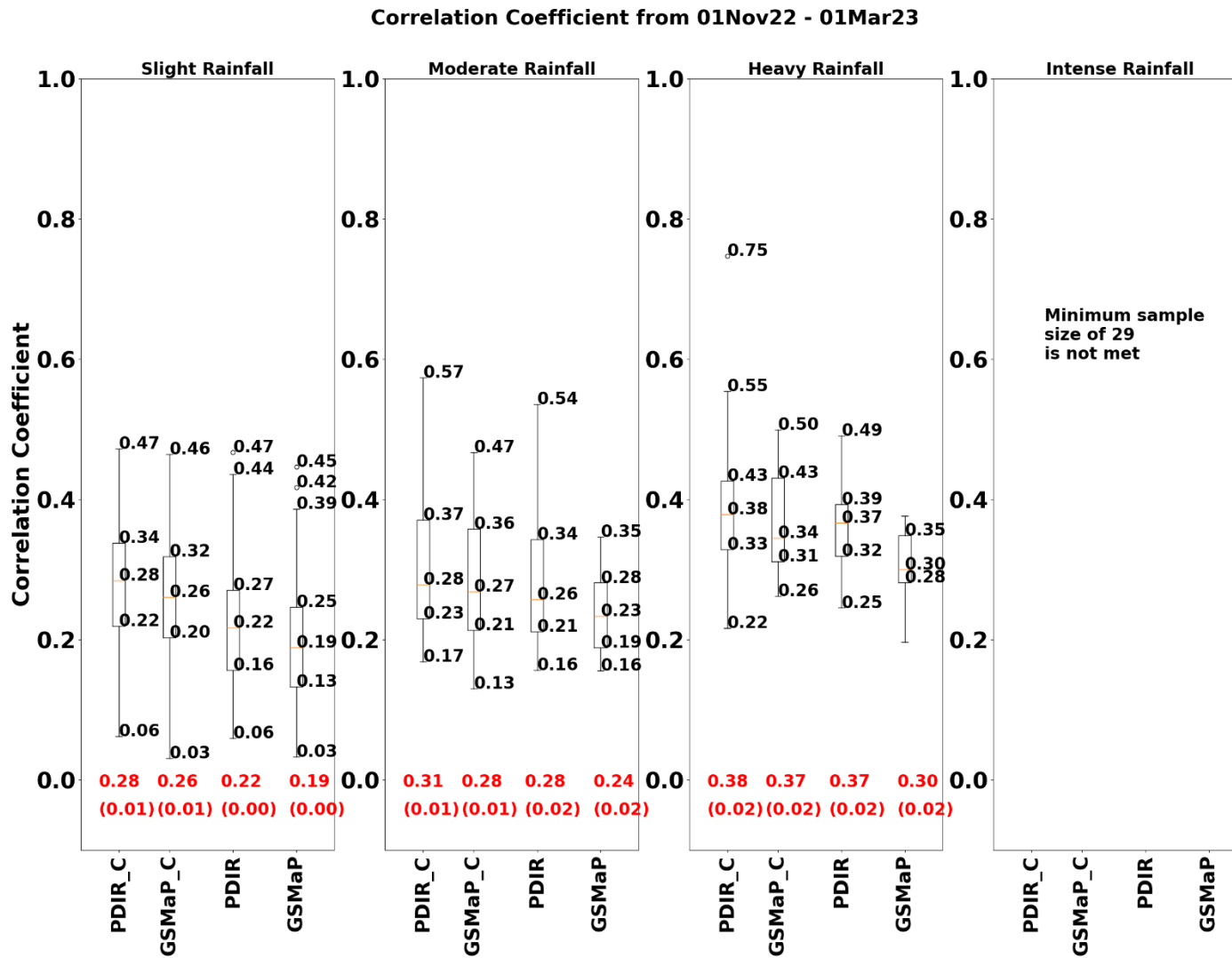
Figure 6. Pearson correlation for hourly rainfall for each category. Average correlation is at the bottom of boxplot and standard error in brackets. Reference for the definition of *slight, moderate, heavy*, and *intense* rainfall is in **Table 4**.

3.2 Analysis of Rainfall Amount and Percentile

The rainfall amount is a crucial input for issuing flood warning. Diakakis (2010) studied rainfall amount observed by a gauge network and proposed that rainfall threshold can be defined above which flooding is highly probable. Huang et al., (2019) reported that rainfall amount (mm) is the primary input for rainfall-runoff models.

Although rainfall amount (mm) in a unit of time (hour or day) is crucial for hydrologists, satellites might not be able to capture the exact rainfall amount as gauge. This is because of error from satellite measurement. A possible source of error in GSMaP include inconsistencies in 0.5h-forward cloud motion with rain motion, in areas of strong wind shear (Kubota et al., 2020).

Satellite cannot capture the exact hourly rainfall amount as gauge. For instance, as clearly depicted in **Figure 8**, the 95th percentile rainfall amount is 16.2 mm per hour (gauge), but for satellite, it is 6.4 mm per hour (PDIR) and 5.7 mm per hour (GSMaP). To solve this issue, the rainfall percentile (%) rather than amount (mm) is used for validation. For example, if gauge showed 50mm of rainfall corresponding to 95th percentile, and satellite measurement at gauge showed 25mm of rainfall corresponding to 95th percentile, then it is considered a hit. The probability of detection (POD) measures the 'hit'. The POD is the proportion of gauge rainfall picked up by satellite (refer to **Section 2.5** for more details on POD).

Figure 9 depicts validation of hourly rainfall using percentile (%). The probability of detecting (POD) gauge rainfall corresponding to the 95th percentile rainfall is just around 0.10 (PDIR_C). Refer to **Figure 9** for a clear illustration. . This indicates that only 10% of gauge rainfall of at least 95th percentile is successfully picked-up by satellite. Without Barnes successive correction, the POD drops to 0.03 (PDIR).The GSMaP showed negligible POD for the 95th percentile rainfall. This implies that satellite performed rather poorly in detecting hourly extreme events.

One reason for poor performance is due to cross-validation. Here, gauges that are used in validation is not involved in correction of the satellite data. The number of gauges to correct satellite data is reduced, leading to lower validation scores. The performance without cross-validation (where gauges used in correction is also involved in validation) is substantially better (not shown). However, cross-validation is important because it represents actual grid points without or in-between gauges.

Consequently, we infer that the inability of satellite measurements to pick up hourly rainfall is not solely because of rainfall amount mismatch between gauge and satellite. Otherwise, the POD for hourly rainfall (in units of percentiles) would not be so poor.

The satellite rainfall may miss rainfall at gauge location. To an extent, Barnes successive correction can alleviate this issue, as indicated by POD tripling to 0.10 for PDIR_C (**Figure 9**).

On the other hand, **Figure 10**. showed that satellite can pick up daily rainfall reasonably well. The probability of detecting (POD) rainfall corresponding to the 95th percentile is around 0.90 (0.65) for PDIR_C (PDIR). The GSMaP fared worse, whereby POD is just 0.35. The satellite performed better for daily rainfall. For example, if satellite missed rainfall at gauge X in hour Y1, the satellite may hit in gauge X in future times of Y1 – Y24. On the other hand, for hourly rainfall, if satellite missed gauge X in hour Y1, it will be counted as a miss, no second chances.

Meanwhile, the False Alarm Ratio (FAR) is proportion of satellite detected rainfall while gauge showed no rainfall. The FAR for daily rainfall is shown in **Figure 11**, which shows considerable false alarms. For example, if there are 15 gauges reporting extreme rainfall (95th percentile), PDIR_C can successfully detect 14 of them (around 90%). However, the PDIR_C also *detected* extreme rainfall events at 70 gauges, out of which only 14 are true (20% are true; 80% false alarms). This implies that PDIR_C (and other satellite datasets which have high FAR as well) may consistently overestimate higher rainfall, as described above.
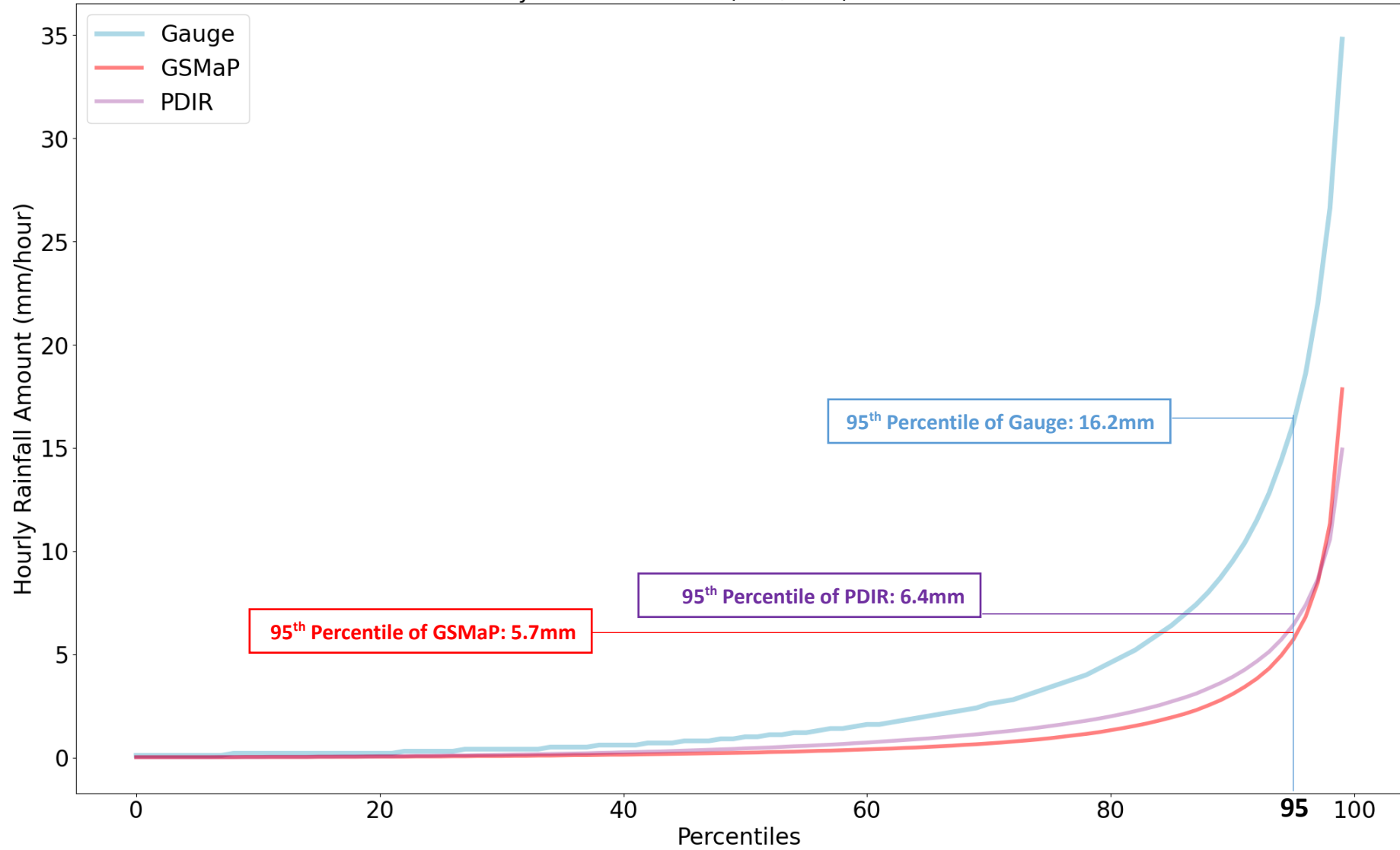
Figure 8. Ranked percentiles of hourly rainfall amount based on 304 gauges from 01 November 2022 – 01 March 2023.
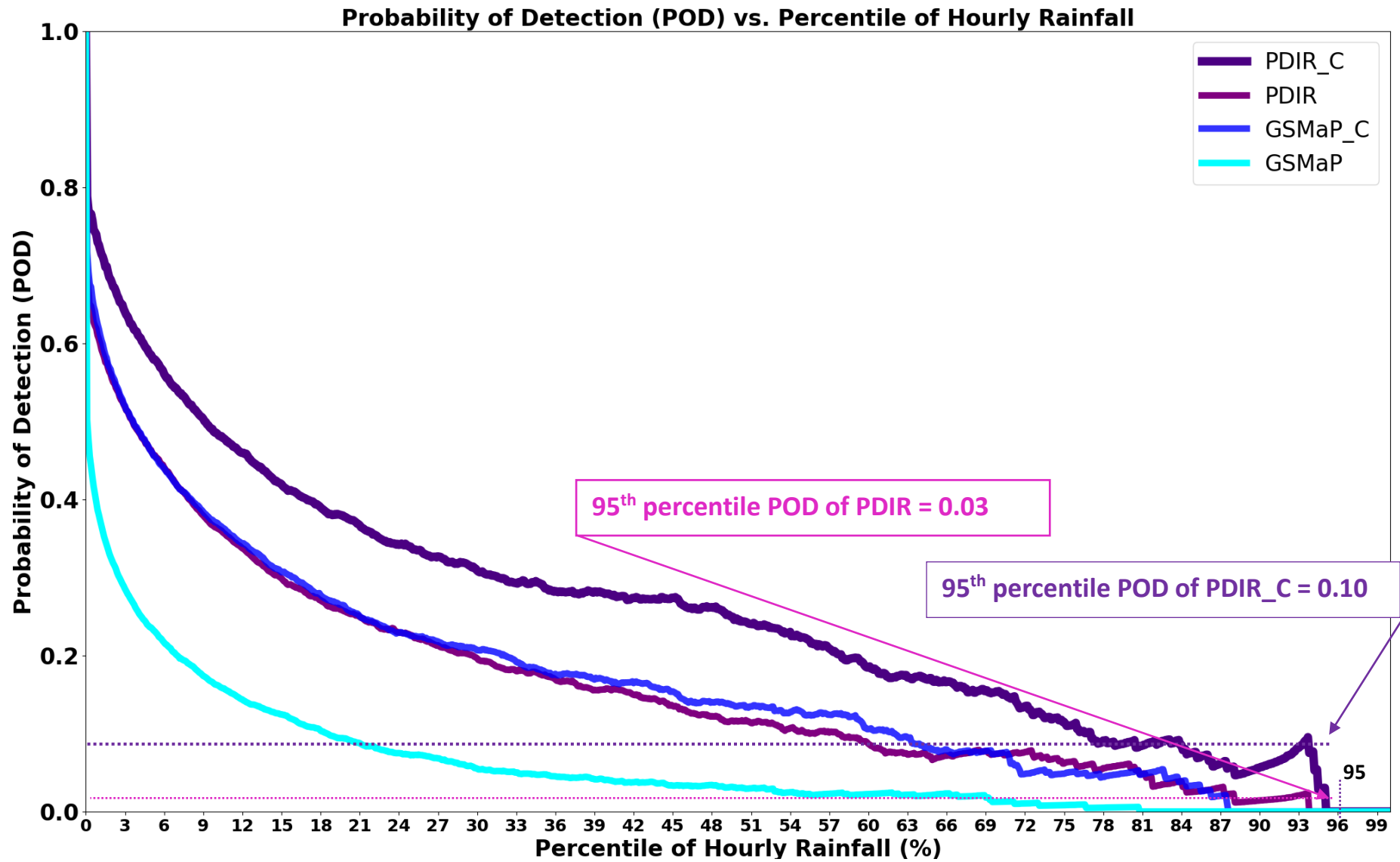
Figure 9. Probability of detection (POD) of satellite hourly rainfall in relation to hourly gauge rainfall; categorized by percentile (%).
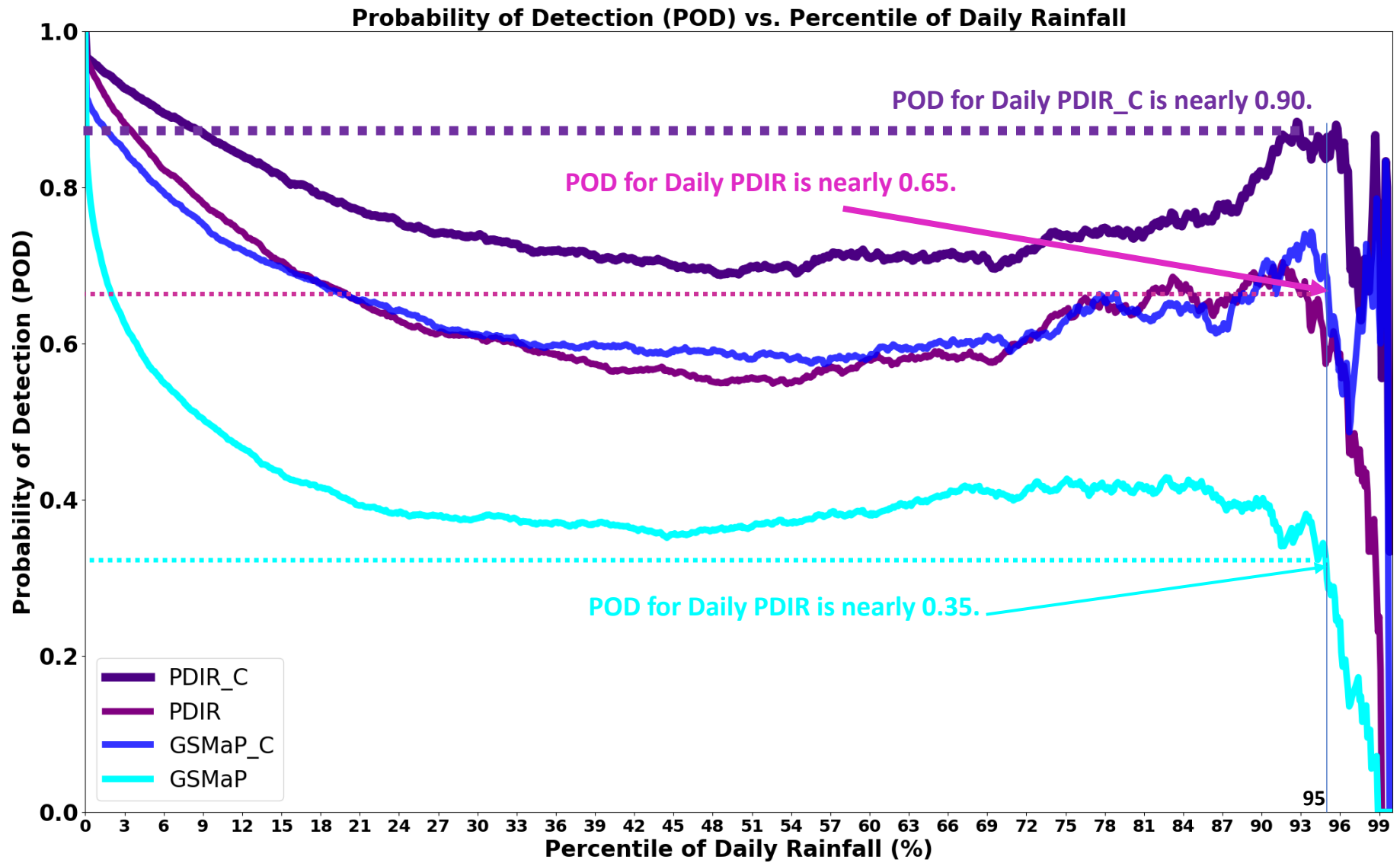
Figure 10. Probability of detection (POD) for satellite daily rainfall in relation to daily gauge rainfall; categorized by percentile (%).
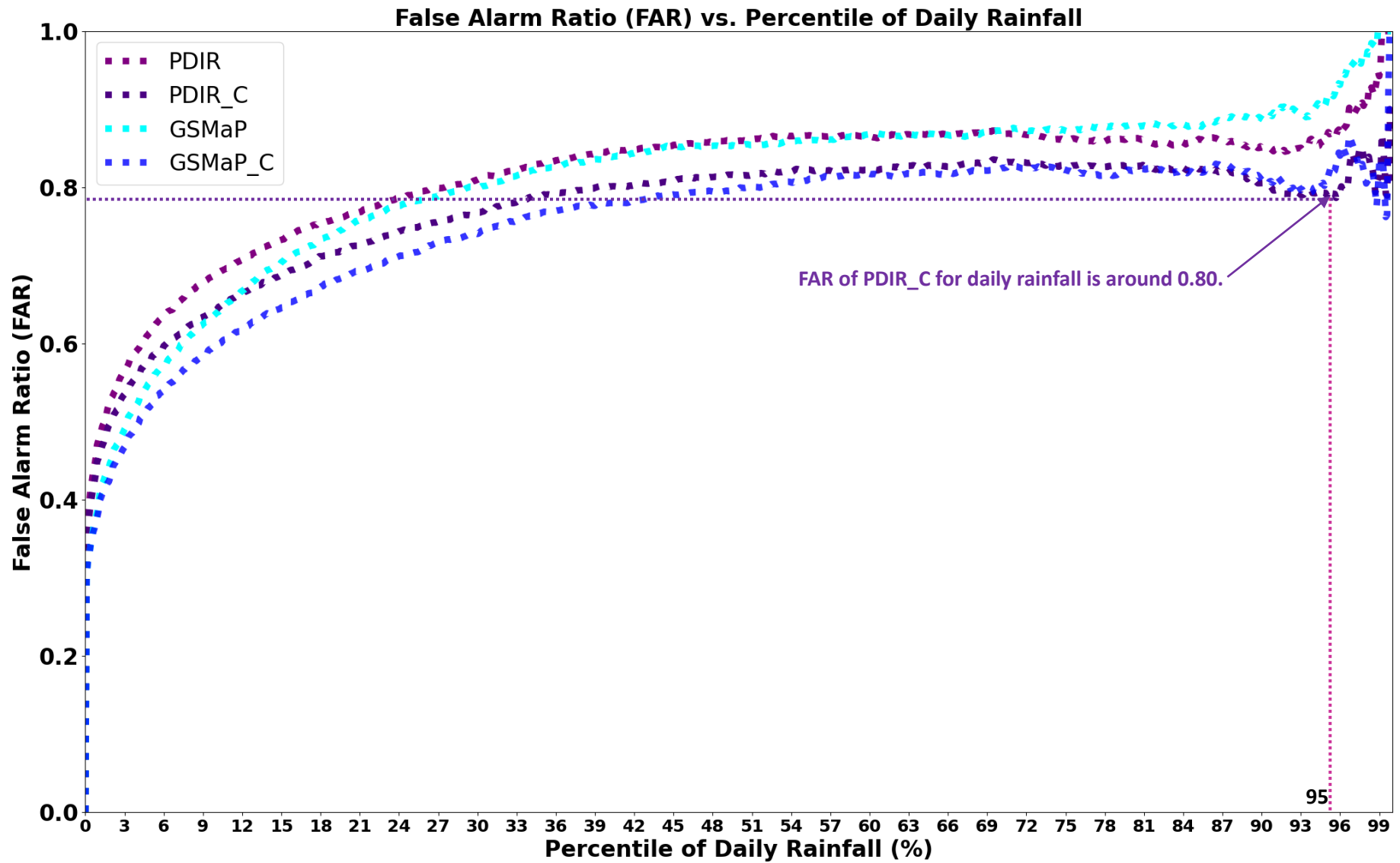
Figure 11. The false alarm ratio (FAR) of satellite daily rainfall in relation to daily gauge rainfall; categorized by percentile.

4. Conclusion

In this study, two satellite rainfall estimation datasets, namely PDIR and GSMaP are evaluated with respect to hourly and daily accumulated rainfall measured by rainfall gauges. The impact of applying Barnes successive correction is also evaluated. The method of evaluation used is ten-fold cross-validation and the metrics of evaluation used are the root-mean-square-error, Pearson correlation coefficient, probability of detection (POD), and false alarm ratio (FAR).

Validation is performed for the overall season (01 Nov 2022 – 01 Mar 2023). Subsequent validation is performed for slight, moderate, heavy, and intense rainfall for the overall season, to determine how well the gridded satellite performs in various types of rainfall. In the overall season and subsequent rainfall categories, it was generally observed that the PDIR has lower rmse compared to GSMaP. Additionally, PDIR has higher co-variability with rainfall gauges because it has higher correlation in relation to gauge, compared to GSMaP. Application of Barnes successive correction further reduces the rmse and increases the correlation of satellite rainfall with respect to gauge.

However, the relatively high rmse for both daily and hourly rainfall confirms that satellite may not necessarily detect the exact amount of rainfall observed by gauges. This may be due to biases in rainfall amount because of satellite errors. To remove the impact of biases in rainfall amount, the rainfall amounts of gauge and satellite are converted to percentiles for categorical validation.

The probability of detection (POD) for hourly rainfall is still low (0.10 for 95th percentile rainfall). It implies that satellite performs poorly in detecting hourly extreme rainfall. A possible cause of error is geometric error (Janowiak et al., 2001) where satellite line of sight is obscured by other clouds. This issue is more acute the further away from the satellite nadir. A possible method of investigating this issue in a future study, is by measuring the POD of extreme rainfall events at gauge, as a function of distance from satellite nadir. It is also important to note if the POD decreases when there are heavy rainfall events between the event and the satellite nadir.

Nevertheless, the POD for daily rainfall is high (around 0.90 detecting for the 95th percentile rainfall gauge rainfall), using PDIR_C. Therefore, the PDIR_C may be more suited for monitoring extreme rainfall (95th percentile) daily rather than hourly basis. It is more suitable for daily climate indices using the 95th percentile daily rainfall.

In addition, the false alarm ratio (FAR) of hourly and daily rainfall is high in PDIR_C, GSMaP_C, GSMaP, and PDIR. A possible cause of higher FAR could be as follows: the

further away from the satellite nadir, the viewing angle is bigger, and clouds are more spread out than if viewed overhead (Janowiak et al., 2001). This may cause larger area of cloud cover than actual. In addition, Infra-red rays suffer more attenuation as the atmospheric optical depth is deeper (Janowiak et al., 2001). It is possible that larger *apparent* cloud coverage and attenuation of IR, leads to cooler IR temperatures for areas far away from the satellite nadir. This corresponds to satellite measuring rainfall that is more intense and widespread than actual, leading to false alarms. This hypothesis can be analysed in further studies. A possible experiment is to measure the false alarm ratio (FAR), rate of change with respect to distance from satellite nadir.

To improve the performance of satellite rainfall measurement, the gauge density can be increased, which allows satellite data to be adjusted with respect to more gauges, via Barnes successive correction. In addition, enhancing the resolution of satellite datasets helps increase detectability of rainfall events. The SEMDP is moving in this direction, for example, the upcoming CMORPH2 near-real-time dataset has 0.05 degrees in resolution, which is about 5km by 5km. This is an improvement from the 8km-by-8km resolution of CMORPH (Xie et al., 2022).

It was shown that for purposes of rainfall monitoring, using PDIR gives higher accuracy in relation to gauges rainfall than GSMaP. Furthermore, applying Barnes successive correction adds to the accuracy (in relation to gauge rainfall), of PDIR and GSMaP. In the case of daily rainfall (rmse, correlation), and hourly rainfall (correlation), the rmse (correlation) is reduced (increased) by nearly one quartile, when Barnes successive correction is applied.

Nonetheless, the accuracy of satellite hourly rainfall amounts in relation to gauges leaves much to be desired, as shown by the high rmse, and low probability of detection (POD). This is true, even when Barnes successive correction is applied. In addition, the satellite tends to overestimate extreme daily rainfall. Further improvements from the present state, such as by increasing the size of the gauge network, and efforts by satellite providers to increase resolution, may close the gap between gauges and satellite rainfall.

References

1. Bujang, M.A., & Baharum, N., (2016). Sample Size Guideline for Correlation Analysis. *World Journal of Social Science Research, 3(1),* 37 – 46. DOI: 10.22158/wjssr.v3n1p37

2. Chen, T.C., Tsay, J.D., Yen, M.C., & Matsumoto, J. (2013). The Winter Rainfall of Malaysia. *Journal of Climate, 26, 936 – 958.* DOI: 10.1175/JCLI-D-12-00174.1

3. Devi, G. K., Ganasri, B. P., & Dwarakish, G. S. (2015). A review on hydrological models. *Aquatic procedia*, *4*, *pp. 1001-1007.* https://doi.org/10.1016/j.aqpro.2015.02.126

4. Diakakis, M. (2012). Rainfall thresholds for flood triggering. The case of Marathonas in Greece. *Natural Hazards, 60,* 789 – 800. https://doi.org/10.1007/s11069-011-9904-7

5. Fakaruddin, F.J. Yip, W.S., Diong, J.Y., Dindang, A., Chang, K.C., & Abdullah, M.H. (2020). Occurrence of meridional and easterly surges and their impact on Malaysian rainfall during the northeast monsoon: a climatology study. *Meteorological Applications, 27(1), e1836.* https://doi.org/10.1002/met.1836

6. Grant, I., Jones, D., Wang, W., Fawcett, R., & David, B. (2008). Meteorological and remotely sensed datasets for hydrological modelling: A contribution to the Australian Water Availability Project. In *Catchment-scale Hydrological Modelling and Data Assimilation (CAHMDA-3) International Workshop on Hydrological Prediction: Modelling, Observation and Data Assimilation, Melbourne, 9-11 January 2008.*

7. Huang, Y., Bardossy, A., & Zhang, K. (2019). Sensitivity of hydrological models to temporary and spatial resolution of rainfall data. *Hydrology and Earth System Sciences, 23 (6),* 2647 – 2663. DOI: 10.5194/hess-23-2647-2019.

8. Janowiak, J.E., Joyce, R.J., & Yarosh, Y. (2001). A Real-Time Global Half-Hourly Pixel-Resolution Infrared Dataset and Its Applications. *Bulletin of the American Meteorological Society, 82 (2),* 205 – 218. DOI: 10.1175/1520-0477 (2001) 082<0205: ARTGHH>2.3.CO;2.

9. Jones, D.A., Wang, W., & Fawcett, R.(2009). High-quality spatial climate data-sets for Australia. *Australian Meteorological and Oceanographic Journal*, *58,* 233-248. http://dx.doi.org/10.22499/2.5804.003

10. Kubota, T., Aonashi, K., Ushio, T., Shige, S., Takayabu, Y., Kachi, M., Arai, Y., Tashima, T., Masaki, T., Kawamoto, N., Mega, T., Yamamoto, M.K., Hamada, A., Yamaji, M., Liu, G., & Oki, R.(2020). Global Satellite Mapping of Precipitation (GSMaP) Products in the GPM Era. In Levizzani., V., Kidd, C., Kirschbaum, D.B., Kummerow, C.D., Nakamura, K., Turk, F.J. (Eds.), *Satellite Precipitation Measurement. Advances in Global Change Research,* 67, 355 – 373. Springer, Cham. Online ISBN: 978-3-030-24568-9. Print ISBN: 978-3-030-24567-2. https://doi.org/10.1007/978-3-030-24568-9_20.

11. Li, Q., Wei, J., Yin, J., Qiao, Z., Peng, W., & Peng, H. (2021). Multiscale Comparative Evaluation of the GPM and TRMM Precipitation Products Against Ground Precipitation Observations over Chinese Tibetan Plateau. *IEEE Journal of Selected Topics in Applied Earth Observations and Remote Sensing, 14,* 2295 – 2313. https://doi.org/10.1109/JSTARS.2020.3047897

12. Liu, C.Y., Aryastana, P., Liu, G.R., & Huang, W.R. (2020). Assessment of satellite precipitation product estimates over Bali Island. *Atmospheric Research 244 (2020) 105032.* https://doi.org/10.1016/j.atmosres.2020.105032

13. Moten, S., Yunus, F., Ariffin, M., Burham, N., Diong, J.Y., Mat Kamaruzaman, M.A., & Yip, W.S.(2014). Statistics of Northeast Monsoon Onset, Withdrawal and Cold Surges in Malaysia. *Guidelines 2014, Malaysian Meteorological Department.* ISBN 978-967-5676-58-1.
    https://ideas.met.gov.my/pub/paper/2014/researchpaper_201400.pdf

14. Nguyen, P., Ombadi, M., Gorooh, V.A., Shearer, E.J., Sadeghi, M., Sorooshian, S., Hsu, K., Bolvin, D., & Ralph, M.F. (2020). Persiann dynamic infrared-rain rate (PDIR-Now): A near-real-time, quasi-global satellite precipitation dataset. *Journal of Hydrometeorology*, 21(12). 2893 – 2906. DOI: 10.1175/JHM-D-20-0177.1

15. Refaeilzadeh, P., Tang, L., & Liu, H.et al., (2016). Cross-Validation. In: Liu, L., Özsu, M. (eds) *Encyclopedia of Database Systems*.2019 - 2023. Springer, New York, NY. https://doi.org/10.1007/978-1-4899-7993-3_565-2

16. Sevruk, B. (2006). Rainfall Measurement: Gauges. In M.G. Anderson and J.J. McDonnell (Ed.) *Encyclopedia of Hydrological Sciences.* John Wiley and Sons, Ltd (15 April 2006). Print ISBN: 9780471491033, Online ISBN: 9780470848944. DOI: 10.1002/0470848944.

17. Sinha, S.K., Narkhedkhar, S.G., & Mitra, A.K.(2006). Barnes objective analysis scheme of daily rainfall over Maharashtra (India) on a mesoscale grid. *Atmosfera, 19(2), pp. 109 – 126*. ISSN 0187-6236.

18. Weymouth, G., Mills, G.A., Jones, D., Ebert, E.E., & Manton, M.J.(1999). A continental-scale daily rainfall analysis system. *Australian Meteorological Magazine*, *48*, 169 – 179. ISSN: 0004-9743. Retrieved from https://www.researchgate.net/publication/285837729_A_continental-scale_daily_rainfall_analysis_system.

19. World Meteorological Organization. (2021a). Chapter 6. Measurement of Precipitation.*Guide to Instruments and Methods of Observation.* 1*, pp. 225*. Retrieved from https://library.wmo.int/doc_num.php?explnum_id=11612.

20. World Meteorological Organization. (2021b). Chapter 14. Observation of Present and Past Weather; State of the Ground. In Guide to Instruments and Methods of Observation (WMO No. 8) Volume 1: Measurement of Meteorological Variables (2021 edition). pp. 517. ISBN: 978-92-63-10008-5. Retrieved from https://library.wmo.int/index.php?lvl=notice_display&id=12407#.XiGSwf5KiUk.

21. World Meteorological Organization. (2022). *Space-based Weather and Climate Extremes Monitoring (SWCEM).* https://public.wmo.int/en/programmes/wmo-space-programme/swcem

22. Xie, P.P., Wu, S., Katz, B., & Sinsky, E. (2022). Second Generation CMORPH for Real-Time Monitoring. VAWS Webinar, 17 August, 2022. NOAA Climate Prediction Center. Retrieved from https://uaf-accap.org/wp-content/uploads/2022/08/VAWS_CMORPH_20220817.pdf